Improving the estimation of human climate influence by selecting appropriate forcing simulations

Chao Li, Zhaoyun Wang, Francis W. Zwiers, & Xuebin Zhang

2021

Original citation:

Li, C., Wang, Z., Zwiers, F., & Zhang, X. (2021). Improving the estimation of human climate influence by selecting appropriate forcing simulations. *Geophysical Research Letters*, *48*(24), e2021GL095500. https://doi.org/10.1029/2021GL095500

AGU ADVANCING EARTH AND SPACE SCIENCE

Geophysical Research Letters

RESEARCH LETTER
10.1029/2021GL095500

Key Points:

- A perfect model analysis to configure climate change detection and attribution analyses before application to observations is suggested
- The best configuration for attributing terrestrial warming uses all-forcing, aerosol-only, and natural-only simulations
- The ~1.5°C terrestrial warming since 1850 results from greenhouse gas induced warming of 1.4–2.3°C offset by aerosol cooling of 0.2–1.2°C

Supporting Information:

Supporting Information may be found in the online version of this article.

Correspondence to:

C. Li,
cli@geo.ecnu.edu.cn

Citation:

Li, C., Wang, Z., Zwiers, F., & Zhang, X. (2021). Improving the estimation of human climate influence by selecting appropriate forcing simulations. *Geophysical Research Letters*, *48*, e2021GL095500. https://doi.org/10.1029/2021GL095500

Received 29 JUL 2021
Accepted 20 NOV 2021

Improving the Estimation of Human Climate Influence by Selecting Appropriate Forcing Simulations

Chao Li[1,2,3], Zhaoyun Wang[1,2], Francis Zwiers[3,4], and Xuebin Zhang[5]

[1]Key Laboratory of Geographic Information Science, Ministry of Education, East China Normal University, Shanghai, China, [2]School of Geographic Sciences, East China Normal University, Shanghai, China, [3]Nanjing University of Information Science and Technology, Nanjing, China, [4]Pacific Climate Impacts Consortium, University of Victoria, Victoria, BC, Canada, [5]Climate Research Division, Environment and Climate Change Canada, Toronto, ON, Canada

Abstract The regression-based optimal fingerprinting is a key tool for quantifying human climate influence. Most studies over the past decade used Coupled Model Intercomparison Project Phase 5 (CMIP5) simulations, limiting fingerprinting regression configuration options. The CMIP6 Detection and Attribution Model Intercomparison Project (DAMIP) provides several types of individual forcing simulations and thus greater configuration flexibility. To avoid overfitting the limited observational data, we suggest that a DAMIP-based perfect model study is first used to best configure the fingerprinting regression prior to its application to observations. We find that a regression using all-forcing, aerosol-only, and natural-only simulations is an overall best option for constraining human-induced global terrestrial warming, which differs from choices commonly made previously. Applying this configuration to observations, we estimate that of the observed terrestrial warming of ~1.5°C between 1850–1900 and 2011–2020, anthropogenic greenhouse gases contributed 1.4 to 2.3°C, offset by aerosol cooling of 0.2 to 1.2°C.

Plain Language Summary To quantify human climate influence, observed climate changes are often regressed onto different forcing responses estimated from climate model simulations. Due to the limited availability of such simulations, most studies over the past decades were restricted in how the regression could be performed. The CMIP6 Detection and Attribution Model Intercomparison Project (DAMIP) provides several types of individual forcing simulations, making it possible to perform the regression in several different ways and raising the question of which is "best". Simply applying different possibilities to the same set of observations to search for the "best" approach could lead to overfitting observations and thus unreliable estimates of human climate influence. We therefore suggest an approach in which the different regression approaches are first applied only to climate model output to determine how to best perform the regression analysis before applying it to observations. Applying the best approach that emerges from studying the climate model output to observations reveals that man-made greenhouse gases contributed 1.4–2.3°C of the observed terrestrial warming of about 1.5°C since the preindustrial period and that aerosols induced an offsetting cooling of 0.2–1.2°C.

1. Introduction

Anthropogenic greenhouse gases and aerosols are the dominant drivers of forced climate change since the preindustrial period (Bindoff et al., 2013). The former has a warming effect by reducing the efficiency with which the Earth emits longwave radiation, while the latter has a net cooling effect through increased scattering of shortwave radiation and changes in aerosol-cloud interactions (Bellouin et al., 2020; Deser et al., 2020). Many detection and attribution studies have estimated their contributions to observed changes in a variety of climate variables at global and regional scales, including mean temperature (e.g., Jones et al., 2013; Najafi et al., 2015; Jones et al., 2016; Gillett et al., 2021; Zhou & Zhang, 2021), mean precipitation (e.g., Zhang et al., 2007; Wu et al., 2013), extreme temperature and precipitation indices (e.g., Seong et al., 2021; Hu et al., 2020; Paik et al., 2020), tropopause height (Santer et al., 2003), human health-related wet bulb globe temperature (Li et al., 2017), and so on.

A 3-signal optimal fingerprinting analysis (e.g., Hegerl et al., 1996; Hasselmann, 1997; Allen & Stott, 2003; Ribes et al., 2013) is often employed to regress an observed climate change onto forced responses to anthropogenic greenhouse gases, other anthropogenic and natural forcings that are directly or indirectly estimated from climate model simulations. Analysis of the fitted regression model (e.g., Jones et al., 2013; Najafi et al., 2015;

Li et al., 2017; Zhou & Zhang, 2021) allows scientists to determine whether the climate-model simulated responses are present in observations, and if so, to estimate the contributions of external forcings to the observed change. Due to the design of the Coupled Model Intercomparison Project Phase 5 (CMIP5; Taylor et al., 2012), most recent studies have formulated the regression model using forcing response signals estimated from all-forcing (ALL), greenhouse gas forcing only (GHG), and natural forcing only (NAT) climate simulations. With this ALL+GHG+NAT signal regression formulation, the effect of AER forcing, or more precisely, other anthropogenic forcing including aerosols and land use changes, is determined by subtraction.

The CMIP6 (Eyring et al., 2016) Detection and Attribution Model Intercomparison Project (DAMIP; Gillett et al., 2016) expanded the availability of different types of externally forced simulations to include anthropogenic aerosols only (AER) as well as GHG, NAT, and ALL, making possible three additional regression analysis configurations: GHG+AER+NAT, ALL+AER+NAT, and ALL+GHG+AER. Almost all studies published since the advent of DAMIP have used the GHG+AER+NAT configuration (e.g., Seong et al., 2021; Hu et al., 2020; Paik et al., 2020), presumably because it avoids having to estimate one of the three principal signals indirectly, as is the case in the other three possible configurations. Whether this choice is optimal remains unknown because uncertainty in the estimation of one signal can affect the detection and attribution of the other signals that enter into the analysis.

The possibility of configuring a fingerprinting strategy in different ways raises a question about how to best configure the fingerprinting regression. This choice, which may be different for different climate variables, should be made independently of the observations so as to avoid overusing, and thus overfitting, the very limited observational resource. Using synthesized observations and forcing simulations via idealized Monte Carlo simulations, Ribes et al. (2015) compared the four fingerprinting configuration strategies and found that ALL+AER+NAT is expected to be the best choice for estimating greenhouse gas-induced warming. This strategy, which in effect allocates more of the climate model simulation effort to the estimation of the weaker signals that enter into the analysis, was recently employed by Gillett et al. (2021) to quantify the relative contributions of anthropogenic greenhouse gases and aerosols to global warming observed since the preindustrial period. Nevertheless, this approach may not be suitable when the forcing responses are estimated from climate models with full complexity or for variables other than global mean temperature.

Here, we present a general perfect model framework based on initial-condition ensemble simulations from a suite of coupled climate models for selecting forcing simulations for separating the contributions of anthropogenic greenhouse gases and aerosols to observed climate changes. We illustrate the approach by considering warming in *global land mean near-surface air temperature* (LSAT) since 1850–1900, but emphasize that it is equally applicable to other climate variables, and thus is expected to offer benefits for accurately estimating human influences on current climate records for monitoring ongoing climate change. We choose LSAT as an illustrative example because land is where the impact of climate warming is felt most directly by humans and because an up-to-date quantification of human influences on terrestrial warming is lacking in the literature.

2. Methods and Data

The 3-signal optimal fingerprinting method for separating the impacts of anthropogenic greenhouse gases and aerosols on LSAT regresses a vector of LSAT observations $\boldsymbol{Y}$ onto the modeled LSAT responses to GHG, AER, and NAT forcings using the total least squares (TLS) algorithm as

$$\boldsymbol{Y} = \beta_{\mathrm{GHG}}\boldsymbol{X}^{*}_{\mathrm{GHG}} + \beta_{\mathrm{AER}}\boldsymbol{X}^{*}_{\mathrm{AER}} + \beta_{\mathrm{NAT}}\boldsymbol{X}^{*}_{\mathrm{NAT}} + \boldsymbol{\varepsilon}_{Y}$$

$$\boldsymbol{X}^{*}_{s} = \boldsymbol{X}_{s} + \epsilon_{s} \quad \text{with } s \text{ denoting GHG, AER, or NAT}$$

where $\boldsymbol{\varepsilon}_{Y}$ represents unforced (internal) variability in $\boldsymbol{Y}$ and $\boldsymbol{\varepsilon}_{s}$ represents errors in the estimates $\boldsymbol{X}^{*}_{s}$ of the true modeled responses $\boldsymbol{X}_{s}$ that result from internal variability simulated by the climate models. Climate model simulations driven by GHG, AER, and NAT forcings are used to estimate these modeled responses via multi-model or multi-member ensemble averaging, as described in more detail later. We estimate the regression coefficients using regularized optimal fingerprinting (Ribes et al., 2013). Fingerprinting strategies where the ALL forcing response is used in place of one of the individual forcing responses, such as in ALL+GHG+NAT, derive the GHG, AER, and NAT regression coefficients through linear transformations of the regression coefficients for

the signals actually included (e.g., Tett et al., 2002; Jones et al., 2013; Najafi et al., 2015; Jones et al., 2016; Li et al., 2017). This assumes that the effects of GHG, AER, and NAT forcings on LSAT are linearly additive, that is, $\boldsymbol{X}_{\mathrm{ALL}} = \boldsymbol{X}_{\mathrm{GHG}} + \boldsymbol{X}_{\mathrm{AER}} + \boldsymbol{X}_{\mathrm{NAT}}$. This assumption is found to be generally valid for mean and extreme temperatures at regional to global scales (e.g., Gillett et al., 2004; Shiogama et al., 2012; Marvel et al., 2015; Wang et al., 2021). Estimates of the contributions of GHG, AER, and NAT forcings to LSAT warming can be calculated based on the estimated regression equation.

We introduce a two-stage procedure for best estimating the contributions of these individual forcings to observed climate change such as LSAT warming. The first stage uses a perfect model approach to select the regression configuration that is likely to be best for detecting and attributing GHG, AER, and NAT forcing responses in observations. This strategy is then applied to the observations in a second stage. The perfect model study stage proceeds as follows. For a given model m with sufficiently large initial-conditions ensembles of each forcing type, we use, in turn, each of the available n_m ALL forcing simulations as pseudo-observations and perform each of the four possible fingerprinting analyses on those pseudo-observations using all other simulations of that model for estimating the necessary forcing responses. By construction, the estimated regression coefficients should concentrate around unity for all external forcings. The extent to which they differ from unity and in their uncertainty can thus be evaluated to identify the best fingerprinting strategy.

For each model m, we measure the accuracy of the estimated regression coefficients for a given external forcing s with the sum of squared errors $\mathrm{SSE}_{s,m} = \sum_{j=1}^{n_m} (\beta_{s,j} - 1)^2$. $\mathrm{SSE}_{s,m}$ is affected by the uncertainty in the estimated forcing response, which depends on the number of available simulations for estimating that response and by uncertainty in the other two forcing responses considered in the regression analysis. This dependence is complex in TLS regression as it depends on individual signal strengths relative to internal variability, the correlation between signals and ensemble size. To ensure that signal strength and intercorrelation are appropriately considered, we define a multi-model weighted average SSE_s where the weight for each model m is determined by the size $n_{m,min}$ of its smallest forcing simulation ensemble so that $\mathrm{SSE}_s = \sum_{m=1}^{M} w_m \mathrm{SSE}_{s,m}$, where $w_m = n_{m,min} / \sum_{j=1}^{M} n_{j,min}$ and M is the number of climate models. That is, more weight is assigned to models that provide forcing response and corresponding regression coefficient estimates with lower sampling uncertainty. We select the fingerprinting strategy for application to observations in the second stage as the one that yields the smallest SSE in the first stage.

Our application of the perfect model approach to LSAT uses monthly mean near-surface air temperature for the 1851–2014 period from 6 CMIP6 climate models with at least 10 ALL forcing simulations and at least 3 individual forcing simulations for GHG, AER, and NAT forcings (CanESM5, CESM2, CNRM-CM6-1, GISS-E2-1-G, IPSL-CM6A-LR, and MIROC6; Table S1 in Supporting Information S1). In order to ensure that the perfect model analysis is as informative as possible for the subsequent realistic analysis with observations, all temperature simulations are processed to emulate the 5°×5° gridded CRUTEM5 data set of observed monthly mean land, air, and temperature anomalies relative to the 1961–1990 climatology (Osborn et al., 2021). Specifically, we convert them to anomalies relative to 1961–1990 on the models' native grid, re-grid the anomalies to the CRUTEM5 grid using bilinear interpolation, mask the re-gridded anomalies by the availability of CRUTEM5 observations, aggregate them to annual mean anomalies for years with at least 9 months of data, compute non-overlapping 5-year means of global land means of these annual mean anomalies for 5-year periods from 1851–1855 to 2011–2014 (with the last period consisting of 4 years), and use them as input for perfect model analysis. Although a perfect model analysis including years after 2014 can be more informative for attributing LSAT warming to date, extending the CMIP6 historical ALL simulations (which end in 2014) to 2020 using, for example, the Shared Socioeconomic Pathway 5-8.5 (SSP5-8.5; O'Neil et al., 2016) simulations would leave only 2 models with the required number of all-forcing simulations, thus limiting the evaluation of multi-model consistency of the selected fingerprinting strategy, which helps to establish confidence in the selection.

We show below that the perfect model study points to ALL+AER+NAT as possibly the best fingerprinting strategy for estimating the influences of GHG, AER, and NAT forcings on LSAT. It is therefore adopted to quantify the contributions of these external forcings to the LSAT warming to date as recorded in CRUTEM5. To that end, we merge the CMIP6 historical ALL simulations for 1851–2014 with the corresponding SSP5-8.5 simulations for 2015–2020 to obtain all-forcing simulations for the whole 1851–2020 period, which is also the period of DAMIP, AER, and NAT simulations. We choose climate models with at least 3 ALL-SSP5-8.5, AER, and NAT simulations (CanESM5, CNRM-CM6-1, FGOALS-g3, HadGEM3-GC31-LL, IPSL-CM6A-LR, and MIROC6; Table S1 in Supporting Information S1), to obtain estimates of forcing responses that are relatively less affected

by internal variability. We note that although the DAMIP and NAT simulations for 2015–2020 are driven by the SSP2-4.5 natural forcing agents (Gillett et al., 2016), using SSP2-4.5 simulations to extend the ALL simulations will reduce the number of available climate models with necessary data, limiting the evaluation of multi-model consistency of the estimated attributable warming. Each simulation is processed as for the perfect model analysis, resulting in non-overlapping 5-year mean LSAT anomalies for 34 5-year periods during 1851–2020. We conduct both individual-model and multi-model fingerprinting analyses. For the former, we estimate the response of LSAT to a particular forcing in a climate model as the ensemble mean of all available simulations for that forcing in that model. For the latter, the response is estimated as the multi-model ensemble mean of the corresponding simulations by averaging all available simulations of each model and then calculating the mean of all available model averages. It should be noted that the TLS fingerprinting method considers internal variability as the single source of error in the estimated model responses and ignores errors that can be induced, for example, by structures and forcing simulation ensemble sizes of different climate models in the multi-model analyses (e.g., Huntingford et al., 2006; Hannart et al., 2014).

The optimal fingerprinting analysis requires two independent estimates of the covariance matrix of internal variability, one for optimizing the signal-to-noise ratio of forcing responses and the other for the residual consistency test. To maximize the number of realizations of internal variability for estimating the covariance matrix, we use preindustrial control simulations from all available CMIP6 climate models as well as inter-ensemble differences of ALL-SSP5-8.5, GHG, AER, and NAT simulations from models with 3 or more ensemble members (as done, for example, Li et al., 2017 and Gillett et al., 2021; Table S1 in Supporting Information S1). It is noted that we use the same covariance matrix estimates for all models studied in the perfect model fingerprinting exercises, precluding the possibility that different configuration choices made with different climate models are due to variations in the estimated covariance matrix.

3. Results and Discussion

3.1. Choosing the Optimal Fingerprinting Strategy by Perfect Model Analysis

Figure 1 presents the estimated GHG, AER, and NAT regression coefficients from perfect model analyses using the four possible fingerprinting strategies implemented on climate models with necessary data. As expected, different strategies lead to different regression coefficient estimates for the same external forcing responses in the same climate models, and thus would produce different estimates of attributable warming with different uncertainties if applied to observations. The GHG+AER+NAT strategy, which has been most heavily used since the advent of the DAMIP simulations, tends to produce biased estimates of some regression coefficients (blue lines in Figure 1). For example, the estimated GHG coefficients in CanESM5 and IPSL-CM6A-LR and NAT coefficients in CNRM-CM6-1, GISS-E2-1-G, and MIROC6 are larger than expected. This is unlikely to have arisen from interactions between external forcings in these climate models as similar overestimation does not emerge when using other fingerprinting strategies, but may be due to the fact that the GHG+AER+NAT forcing combination does not include forcing from stratospheric ozone depletion and land use/cover change. Bias does not seem to affect the ALL+GHG+NAT strategy, which was commonly used in the CMIP5 era, but tends to result in comparatively large regression coefficient uncertainty, particularly for the AER and NAT coefficients (cyan lines in Figure 1).

In contrast, the ALL+AER+NAT and ALL+GHG+AER strategies tend to produce unbiased estimates with lower uncertainties (orange and red lines in Figure 1). On average, based on the multi-model weighted mean SSE of regression coefficient estimates, ALL+AER+NAT performs better in estimating the GHG coefficient, ALL+GHG+AER provides more accurate NAT coefficient estimates, and both have comparable skill in estimating the AER coefficient (orange and red bars in Figure 1). Using idealized Monte Carlo simulations, Ribes et al. (2015) suggested that the ALL+AER+NAT strategy would be the best choice for estimating GHG, AER, and NAT coefficients. This contrast highlights the need to use the available coupled climate model simulations to select the best optimal fingerprinting strategies for particular climate variables. Since international climate policy is focused on anthropogenic climate influence and because the response to natural forcing is generally weak, we take the ALL+AER+NAT strategy as the best overall choice for estimating the contributions of GHG, AER, and NAT forcings to global LSAT warming. It is noted that we obtained qualitatively the same conclusion from a space-time perfect model fingerprinting analysis, which explicitly accounts for the spatial pattern of warming across continents excluding Antarctic (Figure S1 in Supporting Information S1).

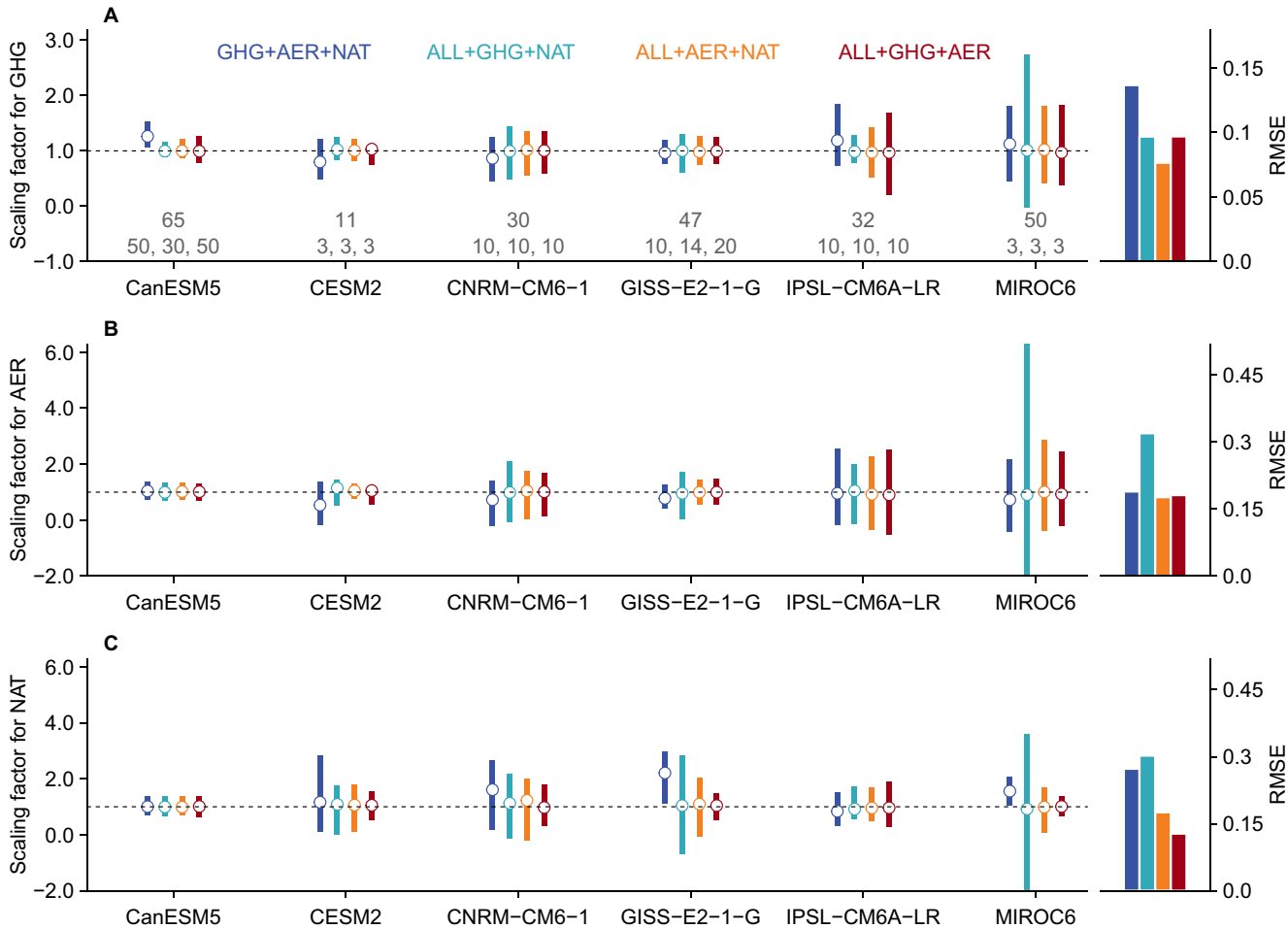

Figure 1. Results of perfect model fingerprinting analyses. Left panels show the estimates of regression coefficients (also known as scaling factors) for GHG (a), AER (b), and NAT (c) forcings obtained with different fingerprinting strategies. Right-hand panels show the root mean squared errors in these regression coefficient estimates, which are computed as the square root of the multi-model mean SSE divided by the total number of all-forcing simulations of these 6 climate models. The numbers in (a) mark the ensemble sizes of ALL, GHG, AER, and NAT simulations of different climate models. Please note the different vertical axis scales in different panels.

To explore why the ALL+AER+NAT strategy stands out, we recall that uncertain regression coefficient estimates can result if multiple correlated responses are involved in a fingerprinting analysis (e.g., Zhang et al., 2013; Li et al., 2017). For a fingerprinting regression model with estimated forcing response matrix $\boldsymbol{X}^*$ and a covariance matrix of forcing response uncertainty due to internal variability $\boldsymbol{S}$, a measure of multicollinearity is the condition number of the matrix $\boldsymbol{L}^{-1/2}\boldsymbol{E}^{\mathrm{T}}\boldsymbol{X}^*$, where $\boldsymbol{L}$ is the diagonal matrix containing the eigenvalues of $\boldsymbol{S}$ and $\boldsymbol{E}$ is the matrix of eigenvectors of $\boldsymbol{S}$. As anticipated, we find that the ALL+AER+NAT strategy shows the weakest multicollinearity among the four possible strategies in all of the climate models considered (Figure S2 in Supporting Information S2). Nevertheless, multicollinearity alone does not provide the full story because severe multicollinearity is found with the second-best ALL+GHG+AER strategy. As mentioned earlier, accurate estimates of forcing responses are critical for obtaining accurate estimates of regression coefficients. Given more or less the same number of simulations, the strong GHG response can be more accurately estimated than the weak NAT response. As a result, the ALL+GHG+AER strategy exhibits similarly good performance as the ALL+AER+NAT strategy even with severe multicollinearity.

Figure 1 also demonstrates that estimation accuracy varies among climate models regardless of fingerprinting strategies. Generally, more accurate estimates of regression coefficients are obtained for climate models having larger numbers of forcing simulations (as marked by numbers in Figure 1a). Nevertheless, one may be curious about why the CESM2 regression coefficient uncertainties are so small given that its individual forcing

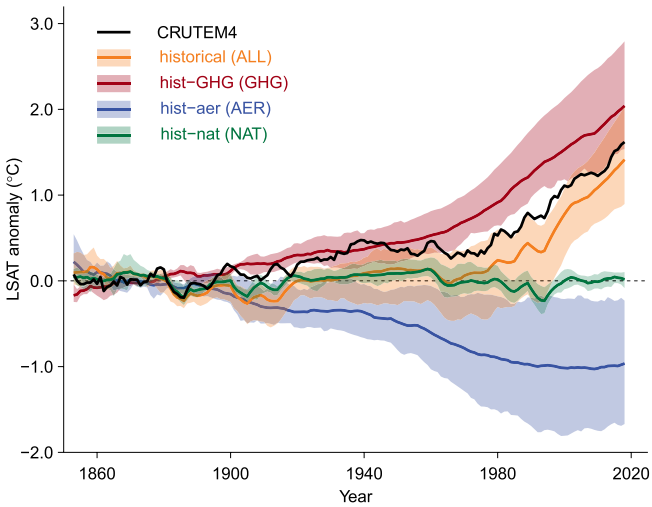

Figure 2. The global land mean near-surface air temperatures from observations and CMIP6 simulations relative to 1851–1900. Observed 5-year running mean LSAT anomalies (black line) are compared with the multi-model mean responses estimated from ALL-SSP5-8.5 (orange line), GHG (red line), AER (blue line), and NAT (green line) simulations from all available CMIP6 climate models that simultaneously have at least 3 simulations for all the forcings considered (CanESM5, CNRM-CM6-1, FGOALS-g3, HadGEM3-GC31-LL, IPSL-CM6A-LR, and MIROC6). Shading marks the ranges of individual model responses.

simulations have only three members, demonstrating a stark contrast with the MIROC6 model, which also has three-member individual forcing ensembles but produces remarkedly more uncertain regression coefficient estimates. One possible explanation is that CESM2 responds more sensitively to external forcings than MIROC6, as indicated by its much higher equilibrium (5.15°C vs. 2.6°C) and transient (1.99°C vs. 1.58°C) climate sensitivities (Zelinka et al., 2020), suggesting that the relative impact of internal variability on forcing response estimates from a small number of simulations will be lower for CESM2.

One could simply rank the fingerprinting strategies according to how well they fit the observations as an alternative to using the perfect model strategy described above, but doing so would likely result in overfitting the observations. We believe that a substantial part of the potential for overfitting can be avoided by first investigating the choice of fingerprinting strategy based purely on climate model simulations, and then only fitting the selected strategy to the observations for a final detection and attribution analysis. The fingerprinting strategies can also be ranked by an imperfect model approach (e.g., Schurer et al., 2018; Gillett et al., 2021). This approach proceeds by first withholding one of the six climate models considered in the perfect model analysis. Each of the available ALL forcing simulations from the withheld model is used in turn as pseudo-observations to perform the four fingerprinting analyses using multi-model mean forcing responses estimated from the remaining models, with which the GHG, AER, and NAT contributions to the warming in the pseudo-observations are estimated. This is repeated for each model, and the resulting collection of warming estimates attributable to each forcing in the climates of each of the models are then compared with the corresponding model-simulated ensemble-mean warming values to choose the best overall fingerprinting strategy. This approach is informative for situations where the observations and models are exchangeable (Annan & Hargreaves, 2010), that is, when the observations are as far from the models as any one model is from all other models being considered. Results (Figure S3 in Supporting Information S3) point to the same ALL+AER+NAT combination as the best overall choice, as obtained from the perfect model approach, although differences among different configurations are not large. In the absence of strong guidance from the imperfect model approach, our perfect model approach provides an objective basis for making the choice that does not involve the use of the observations, and thus the potential to overfit observations by restricting consideration to the main quantifiable source of uncertainty, which is from internal climate variability.

3.2. Constraining the Contributions of External Forcing to LSAT Warming

Adopting the ALL+AER+NAT strategy, we quantify the contributions of GHG, AER, and NAT forcings to the LSAT warming observed since the preindustrial period. We first compare the observed 5-year running means of LSAT for the 1851–2020 period with the corresponding ALL-SSP5-8.5, GHG, AER, and NAT simulations from the CMIP6 climate models that simultaneously have the necessary simulations for these forcings (Figure 2). The LSAT observations show slow warming before about 1940, followed by a hiatus until about 1980, and then rapid warming to date (black line). The ALL-SSP5-8.5 simulations show little warming before 1980 and then a faster-than-observed rate of warming (orange line and shading). Overall, the observed time series lies within the range but close to the upper bound of the individual ALL-SSP5-8.5 simulations, suggesting possible deficiencies of the models in simulating land surface temperatures. The GHG simulations show nearly monotonic warming throughout the period (red line and shading), while the AER simulations exhibit overall cooling (blue lines and shading). By contrast, the NAT simulations present primarily internal variability without evident long-term trends (green line and shading).

The estimated GHG, AER, and NAT regression coefficients and their 5–95% uncertainty ranges are presented in the left panel of Figure 3. We find that the GHG response is robustly detected in observations using forcing response estimates from all the 6 climate models (the uncertainty ranges of the regression coefficients are well

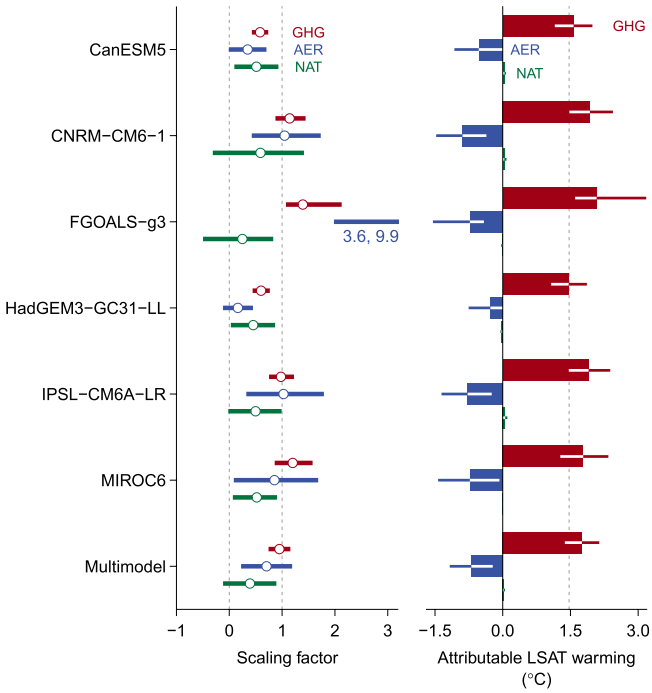

Figure 3. Results of fingerprinting analyses for LSAT warming since the preindustrial period. The left panel shows the best estimates (points) and 5-95% uncertainty ranges (horizontal lines) of GHG, AER, and NAT regression coefficients (also know as scaling factors) using the ALL+AER+NAT fingerprinting strategy selected by intercomparison of perfect model analyses. Right panels show the observed warming in LSAT calculated as the mean difference between 2011–2020 and 1850–1900 (dashed vertical line) and the best estimates of attributed changes (bars) and 5–95% uncertainty ranges (whiskers) for the contributions from GHG, AER, and NAT forcings.

above 0; red lines), as is the AER response when using 5 of the 6 models (blue lines). The NAT response is only detected when using CanESM2 and HadGEM3-GC31-LL (green lines), which have higher equilibrium climate sensitivity than other CMIP6 models (5.64°C and 5.55°C, respectively; Zelinka et al., 2020). Not surprisingly, the GHG and AER responses in these two models are substantially stronger than observed due to their high climate sensitivities (the uncertainty ranges of the regression coefficients are well below 1). We see weaker-than-observed GHG responses when using CNRM-CM6-1, FGOALS-g3, and MIROC6, and AER response when using FGOALS-g3, consistent with their lower climate sensitivities. IPSL-CM6A-LR and CNRM-CM6-1 appear to be most skillful in reproducing the observed responses to both GHG and AER forcings, with regression coefficient estimates essentially equal to one for both signals.

A multi-model analysis using these models (marked "Multimodel" in Figure 3) also identifies robustly detected GHG and AER responses, with the best estimate of the GHG coefficient very close to 1 and the best estimate of the AER coefficient below 1 but with 5–95% uncertainty range that includes 1, meaning that the average GHG response in these models matches the observations closely, while the average AER response is somewhat overestimated but still consistent with the observations. Again, the NAT response is not detected. The estimated regression coefficients for the multi-model mean responses are generally more closely constrained than those for individual-model responses, benefiting from the reduced influence of internal variability on forcing response estimates resulting from multi-model averaging. We note that the residual consistency test is passed in all the above cases, indicating that CMIP6 climate models reasonably reproduce the observed LSAT internal variability.

The estimated contributions of GHG, AER, and NAT forcings to the observed LSAT warming that are inferred from the individual and multi-model analyses are presented in the right panel of Figure 3. According to CRUTEM5, the observed warming in LSAT in the current decade relative to 1850–1900 is about 1.5°C. This is roughly 0.4°C more than the warming in global mean near-surface air temperature over land and oceans combined as reported in Gillett et al. (2021), partly because of the low heat capacity and high Bowen ratio of sensible to latent heat fluxes over land. On the basis of the multi-model analysis with climate models that simultaneously have necessary ALL, AER, and NAT simulations (marked with "Multimodel"), GHG forcing alone is estimated to have caused LSAT warming of 1.8°C (5–95% uncertainty range 1.4°C–2.3°C), which is estimated to have been offset by AER cooling of 0.7°C (0.2°C–1.2°C). The corresponding estimates based on individual models are generally consistent with the multi-model estimates, with the best estimates of GHG- and AER-attributable warming ranging from 1.5°C to 2.1°C and from −0.9°C to −0.5°C, respectively. In all cases, the estimated NAT contributions are negligibly small.

4. Conclusions

In this study, we address the question of how to best use the newly available CMIP6 Detection and Attribution Model Intercomparison Project (DAMIP) simulations to accurately detect and attribute climate changes caused by anthropogenic greenhouse gases and aerosols with a regression-based optimal fingerprinting approach. The availability of several types of DAMIP individual forcing simulations implies that the fingerprinting regression can be configured in several different ways. For example, the historical evolution of global land mean near-surface air temperature (LSAT) can be represented as a linear combination of responses to GHG, AER, and NAT forcing, but can also be represented as linear combinations of ALL forcing simulations, which are driven by a prescribed combination of GHG, AER, and NAT forcing, plus two of the three individual forcing simulations. We suggest a two-stage approach in which a perfect model study is first performed to best configure the fingerprinting analysis, using individual ALL simulations as pseudo-observations, before applying the chosen configuration

to observations. A combination of forcing simulations that performs best in such a perfect model context is expected to perform well in a realistic fingerprinting analysis where the observations are used in place of the all-forcing simulations.

Applying the method to LSAT, we find that the best fingerprinting configuration uses a combination of all-forcing, aerosol-forcing only, and natural-forcing only simulations, which differs from the choices commonly made during the CMIP5 era and since the CMIP6 DAMIP simulations have become available. Based on this finding, we estimate that of the observed LSAT warming of ∼1.5°C between 1850–1900 and 2011–2020, anthropogenic greenhouse gases and aerosols contributed 1.8°C (with the 5–95% uncertainty range from 1.4°C to 2.3°C) and −0.7°C (−1.2°C to −0.2°C), respectively. It should, however, be noted that the best fingerprinting configuration may be different for different climate variables and in different regions and periods and that it will be dependent on the sizes of the available ensembles for single forcing experiments. Also, the best combination may depend on the dimensionality of the signal vectors and how they represent the expected space-time patterns of response to forcing.

The two-stage detection and attribution method that we have proposed and demonstrated is suitable for different climate variables, including many that may be difficult to be modeled by simple Monte Carlo simulations as in Ribes et al. (2015). With the advent of DAMIP, it is now possible to optimize the configuration of a regression-based fingerprinting prior to applying the chosen configuration to observations, thereby substantially avoiding the possibility of overfitting the observations and consequently underestimating detection and attribution uncertainties.

Data Availability Statement

The authors thank the Program for Climate Model Diagnosis and Intercomparison and the World Climate Research Programme's Working Group on Coupled Modeling for making the WCRP CMIP multimodel data set available at https://esgf-node.llnl.gov/search/cmip6/. The CRUTEM5 observations are downloaded from https://www.metoffice.gov.uk/hadobs/crutem5/. This study was supported by the National Key R&D Programs of China (2018YFC1507700, 2020YFA0608901). CL and ZW were also supported by the National Natural Science Foundation of China (42075026).

Acknowledgments
The authors are grateful to Dáithí Stone and an anonymous reviewer for constructive comments on the manuscript. This study was supported by the National Key R&D Programs of China (2018YFC1507700, 2020YFA0608901). CL and ZW were also supported by the National Natural Science Foundation of China (42075026).

References

Allen, M. R., & Stott, P. A. (2003). Estimating signal amplitudes in optimal fingerprinting: I. Theory. *Climate Dynamics*, *21*, 477–491. https://doi.org/10.1007/s00382-003-0313-9

Annan, J. D., & Hargreaves, J. C. (2010). Reliability of the CMIP3 ensemble. *Geophysical Research Letters*, *37*(2), L02703. https://doi.org/10.1029/2009GL041994

Bellouin, N., Quaas, J., Gryspeerdt, E., Kinne, S., Stier, P., Watson-Parris, D., et al. (2020). Bounding global aerosols radiative forcing of climate change. *Review of Geophysics*, *58*, e2019RG000660. https://doi.org/10.1029/2019RG000660

Bindoff, N. L., Stott, P. A., AchutaRao, K. M., Allen, M. R., Gillett, N., Gutzler, D., et al. (2013). Detection and attribution of climate change: From global to regional. In Stocker, T. (Ed.), *Climate Change 2013: The Physical Science Basis* (pp. 867–952). Cambridge University Press.

Deser, D., Phillips, A. S., Simpson, I. R., Rosenbloom, N., Colleman, D., Lehner, F., et al. (2020). Isolating the evolving contributions of anthropogenic aerosols and greenhouse gases: A new CESM large ensemble community resource. *Journal of Climate*, *33*(18), 7835–7858. https://doi.org/10.1175/JCLI-D-20-0123.1

Eyring, V., Bony, S., Meehl, G. A., Senior, C. A., Stevens, B., Stouffer, R. J., & Taylor, K. E. (2016). Overview of the Coupled Model Intercomparison Project Phase 6 (CMIP6) experimental design and organization. *Geoscientific Model Development*, *9*, 1937–1958. https://doi.org/10.5194/gmd-9-1937-2016

Gillett, N. P., Shiogama, H., Funke, B., Hegerl, G., Knutti, R., Matthes, K., et al. (2016). The detection and attribution model intercomparison project (DAMIP v1.0) contribution to CMIP6. *Geoscientific Model Development*, *9*, 3685–3697. https://doi.org/10.5194/gmd-9-3685-2016

Gillett, N. P., Wehner, M. F., Tett, S. F. B., & Weaver, A. J. (2004). Testing the linearity of the response to combined greenhouse gas and surface aerosol forcing. *Geophysical Research Letters*, *31*(14), L14201. https://doi.org/10.1029/2004GL020111

Gillett, N. P., Kirchmeier-Young, M., Ribes, A., Shiogama, H., Hegerl, G. C., Knutti, R., et al. (2021). Constraining human contributions to observed warming since the pre-industrial period. *Nature Climate Change*, *11*, 207–212. https://doi.org/10.1038/s41558-020-00965-9

Hannart, A., Ribes, A., & Naveau, P. (2014). Optimal fingerprinting under multiple sources of uncertainty. *Geophysical Research Letters*, *41*, 1261–1268. https://doi.org/10.1002/2013GL058653

Hasselmann, K. (1997). Multi-pattern fingerprint method for detection and attribution of climate change. *Climate Dynamics*, *13*, 601–611. https://doi.org/10.1007/s003820050185

Hegerl, G. C., von Storch, H., Hasselmann, K., Santer, B. D., Cubasch, U., & Jones, P. D. (1996). Detecting greenhouse-gas-induced climate change with an optimal fingerprint method. *Journal of Climate*, *9*(10), 2281–2306. https://doi.org/10.1175/1520-0442(1996)009<2281:DGGICC>2.0.CO;2

Hu, T., Sun, Y., Zhang, X., Min, S., & Kim, Y. (2020). Human influence on frequency of temperature extremes. *Environmental Research letters*, *15*, 064014. https://doi.org/10.1088/1748-9326/ab8497

Huntingford, C., Stott, P., Allen, M., & Lambert, F. (2006). Incorporating model uncertainty into attribution of observed temperature change. *Geophysical Research Letters*, *33*, L05710. https://doi.org/10.1029/2005GL024831

Jones, G. S., Stott, P. A., & Christidis, N. (2013). Attribution of observed historical near surface temperature variations to anthropogenic and natural causes using CMIP5 simulations. *Journal of Geophysical Research: Atmospheres*, *118*, 4001–4024. https://doi.org/10.1002/jgrd.50239

Jones, G. S., Stott, P. A., & Mitchell, J. F. B. (2016). Uncertainties in the attribution of greenhouse gas warming and implications for climate prediction. *Journal of Geophysical Research: Atmospheres*, *121*(12), 6969–6992. https://doi.org/10.1002/2015JD024337

Li, C., Zhang, X., Zwiers, F. W., Fang, Y., & Michalak, A. M. (2017). Recent very hot summers in northern hemispheric land areas measured by wet bulb globe temperature will be the norm within 20 years. *Earth's Future*, *5*(12), 1203–1216. https://doi.org/10.1002/2017EF000639

Marvel, K., Schmidt, G. A., Shindell, D., Bonfils, C., LeGrande, A. N., Nazarenko, L., & Tsigaridis, K. (2015). Do responses to different anthropogenic forcings add linearly in climate models. *Environmental Research Letters*, *10*, 104010. https://doi.org/10.1088/1748-9326/10/10/104010

Najafi, M. R., Zwiers, F. W., & Gillett, N. P. (2015). Attribution of Arctic temperature change to greenhouse-gas and aerosol influences. *Nature Climate Change*, *5*, 246–249. https://doi.org/10.1038/nclimate2524

Osborn, T. J., Jones, P. D., Lister, D. H., Morrie, C. P., Simpson, I. R., Winn, J. P., et al. (2021). Land surface air temperature variations across the global updated to 2019: The CRUTEM5 data set. *Journal of Geophysical Research - Atmospheres*, *126*(2), e2019JD032352. https://doi.org/10.1029/2019JD032352

Paik, S. S., Min, X., Zhang, M. G., Donat, A. D., King, Sun, Q., & Sun, Q. (2020). Determining the anthropogenic greenhouse gas contribution to the observed intensification of extreme precipitation. *Geophysical Research Letters*, *46*, e2019GL086875. https://doi.org/10.1029/2019GL086875

Ribes, A., Gillett, N. P., & Zwiers, F. W. (2015). Designing detection and attribution simulations for CMIP6 to optimize the estimation of greenhouse gas-induced warming. *Journal of Climate*, *28*(8), 3435–3438. https://doi.org/10.1175/jcli-d-14-00691.1

Ribes, A., Planton, S., & Terray, L. (2013). Application of regularized optimal fingerprinting to attribution. Part I: Method, properties and idealized analysis. *Climate Dynamics*, *4*, 2817–2836. https://doi.org/10.1007/s00382-013-1735-7

Santer, B. D., Wehner, M. F., Wigley, T. M. L., Sausen, R., Meehl, G. A., Taylor, K. E., et al. (2003). Contributions of anthropogenic and natural forcing to recent tropopause height changes. *Science*, *301*(5632), 479–483. https://doi.org/10.1126/science.1084123

Schurer, A., Hegerl, G., Ribes, A., Polson, D., Morice, C., & Tett, S. (2018). Estimating the transient climate response from observed warming. *Journal of Climate*, *31*(20), 8645–8663. https://doi.org/10.1175/JCLI-D-17-0717.1

Seong, M., Min, S., Kim, Y., Zhang, X., & Sun, Y. (2021). Anthropogenic greenhouse gas and aerosol contributions to extreme temperature changes during 1951-2015. *Journal of Climate*, *34*(3), 857–870. https://doi.org/10.1175/JCLI-D-19-1023.1

Shiogama, H., Stone, D. A., Nagashima, T., Nozawa, T., & Emori, S. (2012). On the linear additivity of climate forcing-response relationships at global and continental scales. *International Journal of Climatology*, *33*(11), 2542–2550. https://doi.org/10.1002/joc.3607

Taylor, K. E., Stouffer, R. J., & Meehl, G. A. (2012). An overview of CMIP5 and the experiment design. *Bulletin of the American Meteorological Society*, *93*, 485–498. https://doi.org/10.1175/BAMS-D-11-00094.1

Tett, S. F., Jones, G. S., Stott, P. A., Hill, D. C., Mitchell, J. F., Allen, M. R., et al. (2002). Estimation of natural and anthropogenic contributions to twentieth century temperature change. *Journal of Geophysical Research – Atmospheres*, *107*(D16), ACL101–ACL1024. https://doi.org/10.1029/2000JD000028

Wang, Z., Jiang, Y., Wan, H., Yan, J., & Zhang, X. (2021). Toward optimal fingerprinting in detection and attribution of changes in climate extremes. *Journal of the American Statistical Association*, *116*(533), 1–13. https://doi.org/10.1080/01621459.2020.1730852

Wu, P., Christidis, N., & Stott, P. (2013). Anthropogenic impact on Earth's hydrological cycle. *Nature Climate Change*, *3*, 807–810. https://doi.org/10.1038/nclimate1932

Zelinka, M. D., Myers, T. A., McCoy, D. T., Po-Chedley, S., Caldwell, P. M., Ceppi, P., et al. (2020). Causes of higher climate sensitivity in CMIP6 models. *Geophysical Research Letters*, *47*, e2019GL085782. https://doi.org/10.1029/2019GL085782

Zhang, X., Wan, H., Zwiers, F. W., Hegerl, G. C., & Min, S. (2013). Attributing intensification of precipitation extremes to human influence. *Geophysical Research Letters*, *40*(19), 5252–5257. https://doi.org/10.1002/grl.51010

Zhang, X., Zwiers, F. W., Hegerl, G. C., Lambert, F. H., Gillett, N. P., Solomon, S., et al. (2007). Detection of human influence on 20th century precipitation trends. *Nature*, *448*, 461–465. https://doi.org/10.1038/nature06025

Zhou, T., & Zhang, W. (2021). Anthropogenic warming of Tibetan Plateau and constrained future projection. *Environmental Research Letters*, *16*, 044039. https://doi.org/10.1088/1748-9326/abede8